Shape memory behavior and recovery force of 4D printed laminated Miura-origami structures subjected to compressive loading

Yang Liu[a,b], Wei Zhang[a], Fenghua Zhang[c], Xin Lan[c], Jinsong Leng[c], Shuang Liu[d], Xinqiao Jia[d], Chase Cotton[e], Baozhong Sun[a], Bohong Gu[a,*], Tsu-Wei Chou[b,**]

[a] College of Textiles, Donghua University, Shanghai 201620, PR China
[b] Department of Mechanical Engineering, Center for Composite Materials, University of Delaware, Newark, DE 19716, USA
[c] Center for Composite Materials and Structures, Harbin Institute of Technology, Harbin 150080, PR China
[d] Department of Materials Science and Engineering, University of Delaware, Newark, DE 19716, USA
[e] Department of Electrical and Computer Engineering, University of Delaware, Newark, DE 19716, USA

A B S T R A C T

Four-dimensionally (4D) printed origami structures have great potential for applications in actuators and re-configurable devices by taking the advantages of 3D printing technology and shape memory polymers. This study focuses on the shape recovery progression of 4D printed laminated Miura-origami tessellations and tubes under compressive load-induced unfolding and folding. Recovery forces of the specimens are characterized by dynamic mechanical analysis (DMA) experiments. The shape recovery behavior and recovery force are significantly influenced by the shape recovery temperature and loading pattern. The high shape recovery capability of the specimens are signified by the shape recovery ratio of over 94% and volume changes of up to 289%. Lastly, the actuator application of a 4D printed laminated Miura-origami structure has been demonstrated.

1. Introduction

Origami, which probably originated with the invention of paper in China and refined in Japan [1], is an ancient art of paper folding of crease patterns on a two dimensional (2D) sheet to form complicated three dimensional (3D) structures. The richness of crease patterns of origami has led to the development of variations from zero-curvature classic Miura-origami tessellation [2], single-curvature Miura-origami derivatives [3] and double-curvature origami tessellations [4] to multi-curvature origami Stanford bunny [5]. During the folding process, origami structures exhibit excellent properties, such as shape-changing, negative Poisson's ratio and bistability [6,7]. Origami structures have wide applications in mechanical metamaterials [8,9], artificial muscles [10] and space-saving rocketry [11]. Miura-origami, one of the simplest and most extensively applied origami structures, is constructed using four parallelogram panels with mountain folding and valley folding as defined in section 2. Miura-origami tessellation and tube are capable to build metamaterials with intriguing mechanical property [8,9]. Therefore, Miura-origami tessellation and tube structures are chosen to be studied in this work.

Three-dimensional (3D) printing, commonly known as additive manufacturing, has attracted considerable attention in recent years among scientists and engineers due to its flexibility in fabrication of objects with complex structures [12,13]. Furthermore, by taking the advantages of 3D printing technology and smart materials, 4D printing was first introduced by Tibbits in 2013 [14]. The shape and property of a 4D printed laminated structure usually change over time under external stimuli such as heat [15–17], light [18], water [19,20], electric field [21] and magnetic field [22]. 4D printing technology has been adopted in a broad range of engineering applications from biomedical scaffolds [23], medical device [24], electronic device [25] to dynamic jewelry [26] and smart textiles [27].

Shape memory polymer (SMP), especially heat-actuated SMP, is one of the most commonly used stimulus-responsive materials for actuators and reconfigurable structures. Significant research effort has also been devoted to the study of the shape morphing/recovery behavior of simple and complicated structures based on a single material or multiple materials. For example, Manen et al. [28] presented a new shape-shifting technique that required only a hobbyist 3D printer and a single SMP material. Yu et al. [29] utilized the 3D printing of multiple SMP materials for controlling shape changing sequence. Teoh et al. [30] demonstrated the multi-stage sequential shape recovery process of 4D

---

* Corresponding author.
** Corresponding author.
   E-mail addresses: gubh@dhu.edu.cn (B. Gu), chou@udel.edu (T.-W. Chou).
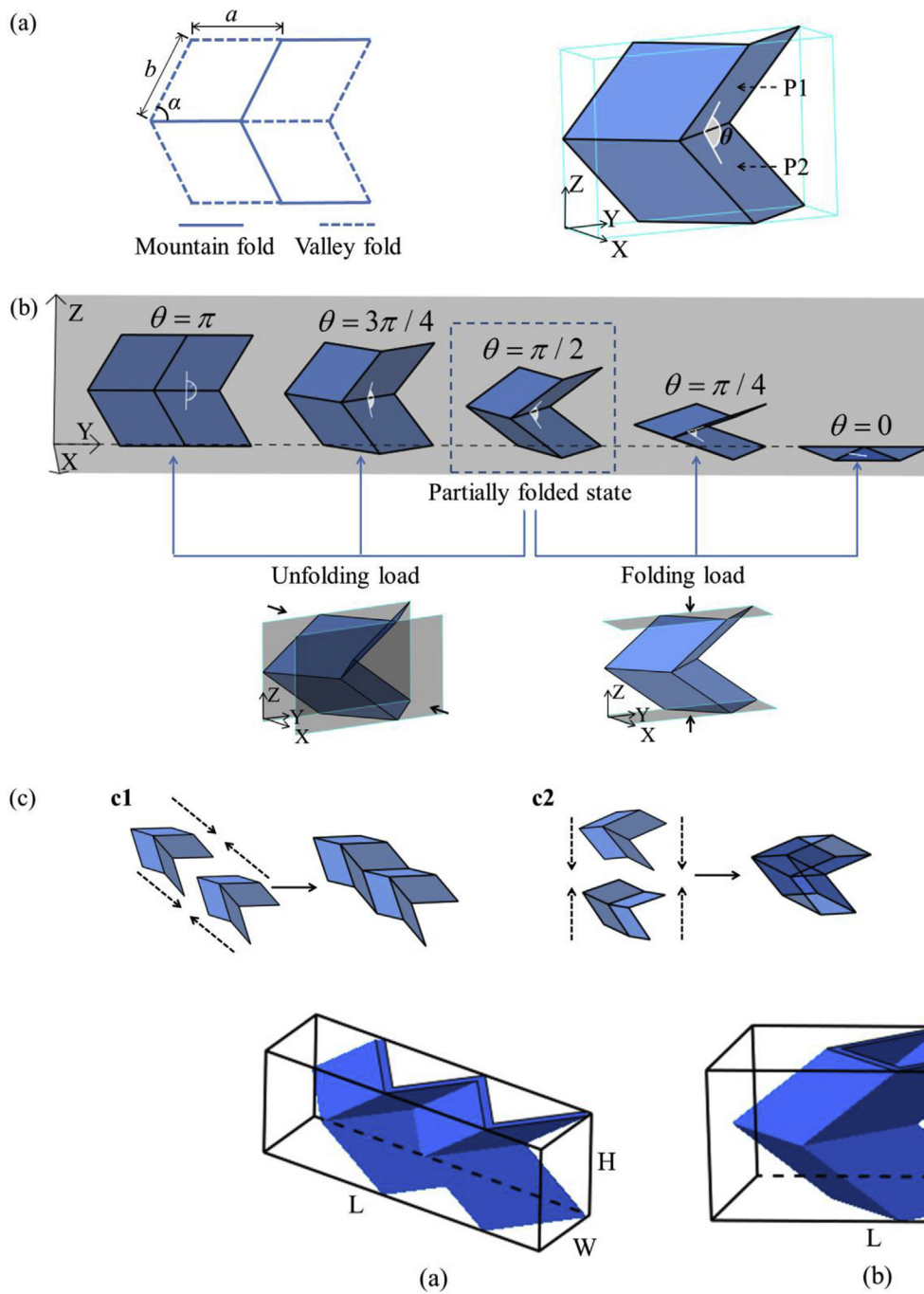
Fig. 1. Geometric definitions and variations of the Miura-origami structure. (a) The 2D crease pattern (left) of a Miura-origami unit cell is defined by the vertex angle α, and the sides a and b. A partially folded unit cell (right) is defined by its dihedral angle θ between the facets P1 and P2. (b) The variations of folded states of a Miura-origami unit cell with the dihedral angles. Fully unfolded state and fully folded state are shown with the dihedral angles of π and 0, respectively. When the unit cell is partially folded, the unit cell can be deformed by unfolding load and folding load applied perpendicular to the Y-Z plane and X-Y plane, respectively. (c) The Miura-origami tessellation can be formed by joining two unit cells in series (c1) while the Miura-origami tube can be formed by joining two unit cells as mirror-images of each other (c2).

Fig. 2. The models of thin-walled Miura-origami (a) tessellation and (b) tube. The volumes of the tessellation and tube are defined by the rectangular volume (L × W × H).

printed structures using a single SMP with varying geometric thickness. Bodaghi et al. [31] found that 1D/2D structures printed by fused decomposition modeling (FDM) using SMP could show self-folding or/and self-coiling to 2D/3D structures. Ge et al. [32] developed an intelligent hinge using SMP fibers printed in an elastomeric matrix. Following this approach, Yuan et al. [33] demonstrated the fabrication of complicated origami structures using varying fiber orientations of the intelligent hinge. Wagner et al. [17] studied the large shape transformation of 4D printed auxetic structures with area changes up to 200%. Teoh et al. [34] preliminarily investigated the effect of folding axis and hinge thickness on the cross-folding recovery behavior of 4D printing origami structures. Furthermore, there have been some studies focusing on free shape recovery property and constrained shape recovery property of

SMP non-printing or printing structures subjected to tensile [35,36], compressive [37] and bending [38] load. It can be concluded from the above review that there were very few studies focused on the shape recovery property of 4D single-material printed Miura-origami tessellations and tubes subjected to compressive loading.

In this work, the geometric definitions and variations of Miura-origami structures were first presented. Then, the thin-walled Miura-origami tessellations and tubes were designed and successfully fabricated by fused deposition modeling using SMP filament. Free shape recovery properties and constrained shape recovery properties of 4D printed laminated Miura-origami tessellations and tubes were characterized. The effects of the shape recovery temperature and loading types on the shape memory properties were investigated. Volume changes with the
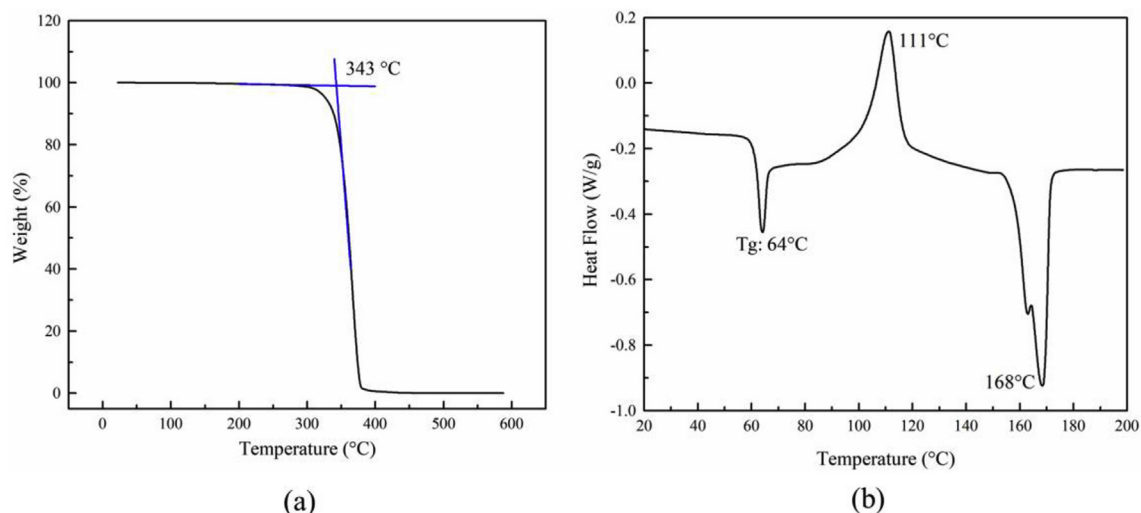
Fig. 3. Thermal properties measurements of PLA based SMP filament. (a) TGA curve (b) DSC curve.

shape recovery process were also determined.

2. Geometric definitions and variations of Miura-origami

The unit cell of a Miura-origami is comprised of four identical parallelogram panels, which are defined by the vertex angle α, and the sides a and b (Fig. 1a). The degree of folding of a unit cell is determined by the dihedral angle θ. By changing θ from π to 0, the degree of folding of the unit cell varies from the fully unfolded state to the fully folded state (Fig. 1b). When the unit cell is partially folded, the unit cell can be deformed by unfolding load and folding load applied perpendicular to the Y-Z plane and X-Y plane, respectively. This is consistent with Mousanezhad's definition [39]. Furthermore, the volumes of Miura-origami structures obviously vary with the different degree of folding state. By combining two unit cells in series, a Miura-origami tessellation can be formed. Likewise, by arranging two unit cells in a mirror-image symmetric pattern, a Miura-origami tube can be formed (Fig. 1c). These two structures were chosen for further studies.

3. Materials and methods

3.1. Material and thermal property measurements

The polylatic acid (PLA) based SMP filament used in fused deposition modeling was fabricated at the Harbin Institute of Technology (HIT). The thermal properties of PLA based SMP filament were investigated using the thermal gravimetric analysis (TGA) measurements under nitrogen atmosphere using a Q600 TGA/DSC (TA Instruments) from room temperature to around 600 °C with ramp rate of 10 °C/min. The sample weight was about 10 mg. The differential scanning calorimetry (DSC) measurements were also performed using a Discovery DSC (TA Instruments) from room temperature to 200 °C with ramp rate of 10 °C/min. The sample weight was about 4 mg.

3.2. Specimen fabrication

The models of thin-walled Miura-origami tessellations and tubes were established by the CATIA software (Fig. 2). The unit cell geometric parameters of tessellation and tube were identical, namely, $a = b = 10$ mm, $\alpha = \pi/3$ and $\theta = \pi/2$. The wall thickness of all specimens is around 0.7 mm. The volumes of the tessellation and tube were defined by the rectangular volume (L × W × H). The sizes of the tessellation and tube are 34.7 (L) × 9.3 (W) × 12.3 (H) mm³ and 23.0 (L) × 18.5 (W) × 12.3 (H) mm³, respectively. Based on the geometric

parameters, the origami tessellation and tube were printed by fused deposition modeling using the PLA based SMP filament. The printing temperature of the nozzle was 200 °C and the printing speed was 50 mm/s.

3.3. Shape memory behavior characterization

The free shape recovery property and constrained shape recovery property of Miura-origami tessellations and tubes have been studied. The characterization of free shape recovery property was carried out in an oven at the recovery temperature without any constraint. The evolution of shape recovery was recorded using a video camera (Sony FDR-AX100); two reference points were used to calculate the change of specimen height. The start of recovery process was defined as the moment when a specimen was placed in an oven at the recovery temperature. The end of recovery process was defined as the moment when the specimen shape no longer showed any noticeable change. The characterization of constrained shape recovery property of the deformed specimen, on the other hand, was carried out with constrained displacement for maintaining a compressive strain around 60%. For this process, the shape recovery force was characterized using RSA-G2 DMA (TA Instruments) with compressive oscillatory temperature ramp from 25 °C to 90 °C at the ramp rate of 5 °C/min. About 0.01 N pre-load was applied to ensure contact between the sample and the parallel plates. The oscillatory strain was set to be 0.1% and the oscillatory frequency was 1 Hz. Zhang et al. [40] used the same method to measure the recovery force of the 4D printed circular braided preform and its composites. All results were recorded from the second shape recovery cycle in order to avoid the influence of heating history. Three specimens were used for every test.

4. Results and discussion

4.1. Thermal properties of the SMP filament

TGA and DSC measurements of the SMP filament were conducted to identify the nozzle temperature for printing. As shown in Fig. 3a, the thermal decomposition temperature of PLA based SMP filament was around 343 °C, which is considered as a limiting processing temperature for the filament. Other thermal parameters are shown in the DSC curve of Fig. 3b. The glass transition temperature (T_g) of the SMP filament was around 64 °C, the crystallization temperature was around 111 °C and the melting temperature was around 168 °C. The T_g, crystallization temperature and melting temperature are close to those
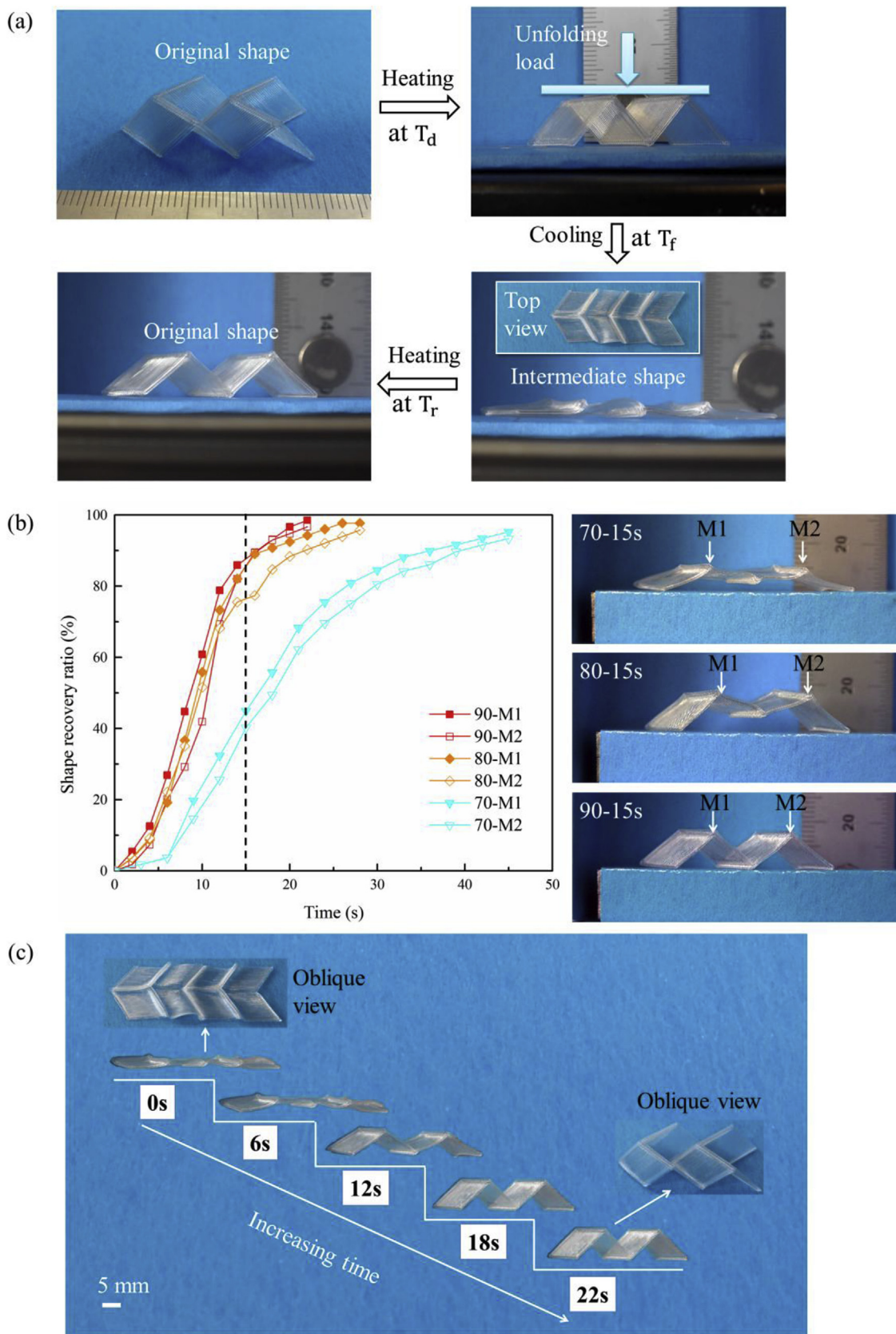
Fig. 4. Shape recovery behavior of a 4D printed Miura-origami tessellation subjected to an unfolding load. (a) Shape recovery cycle. (b) Shape recovery ratio vs. time curves for recovery temperatures of 70 °C, 80 °C and 90 °C. The black dash line indicates the shape recovery time of 15 s. The photographs of specimens at 15 s for the different recovery temperatures are shown on the right. (c) Front view images of the shape recovery process of a specimen at 90 °C. Oblique views of the specimen at 0 s and 22 s are also shown.
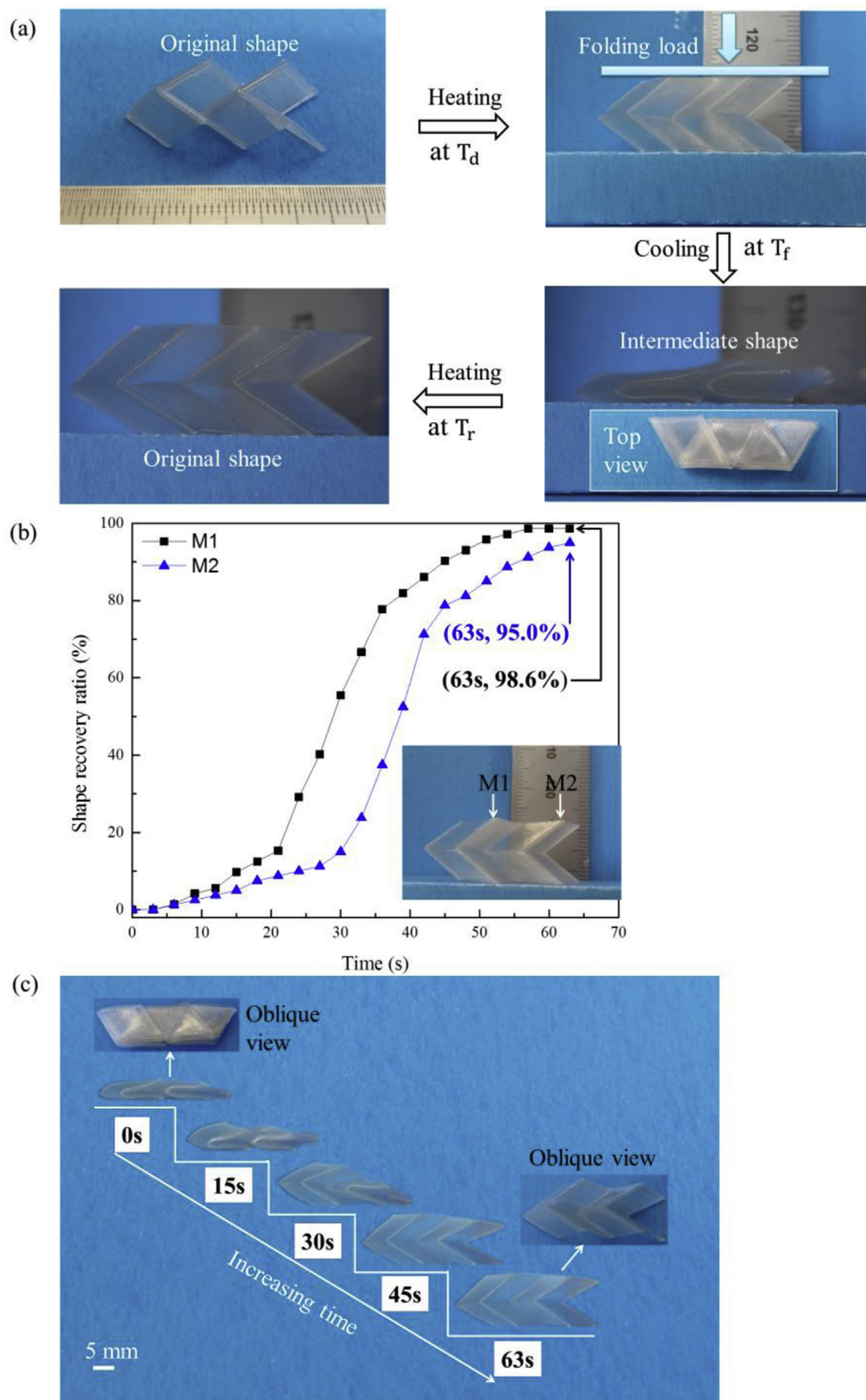
Fig. 5. Shape recovery behavior of a 4D printed Miura-origami tessellation subjected to a folding load. (a) Shape recovery cycle. (b) Shape recovery ratio vs. time curves for the heights of points M1 and M2. (c) Front view images of the shape recovery process of a specimen at 90 °C. Oblique views of the specimen at 0 s and 63 s are also shown.

temperatures of PLA in Senatov's work [37]. Based on the SMP filament thermal properties identified above, the nozzle temperature of 200 °C was chosen for Miura-origami specimen fabrication using fused deposition modeling. In the subsequent study of shape recovery behavior,

the deformation temperature and the shape recovery temperature were chosen to be above T_g.
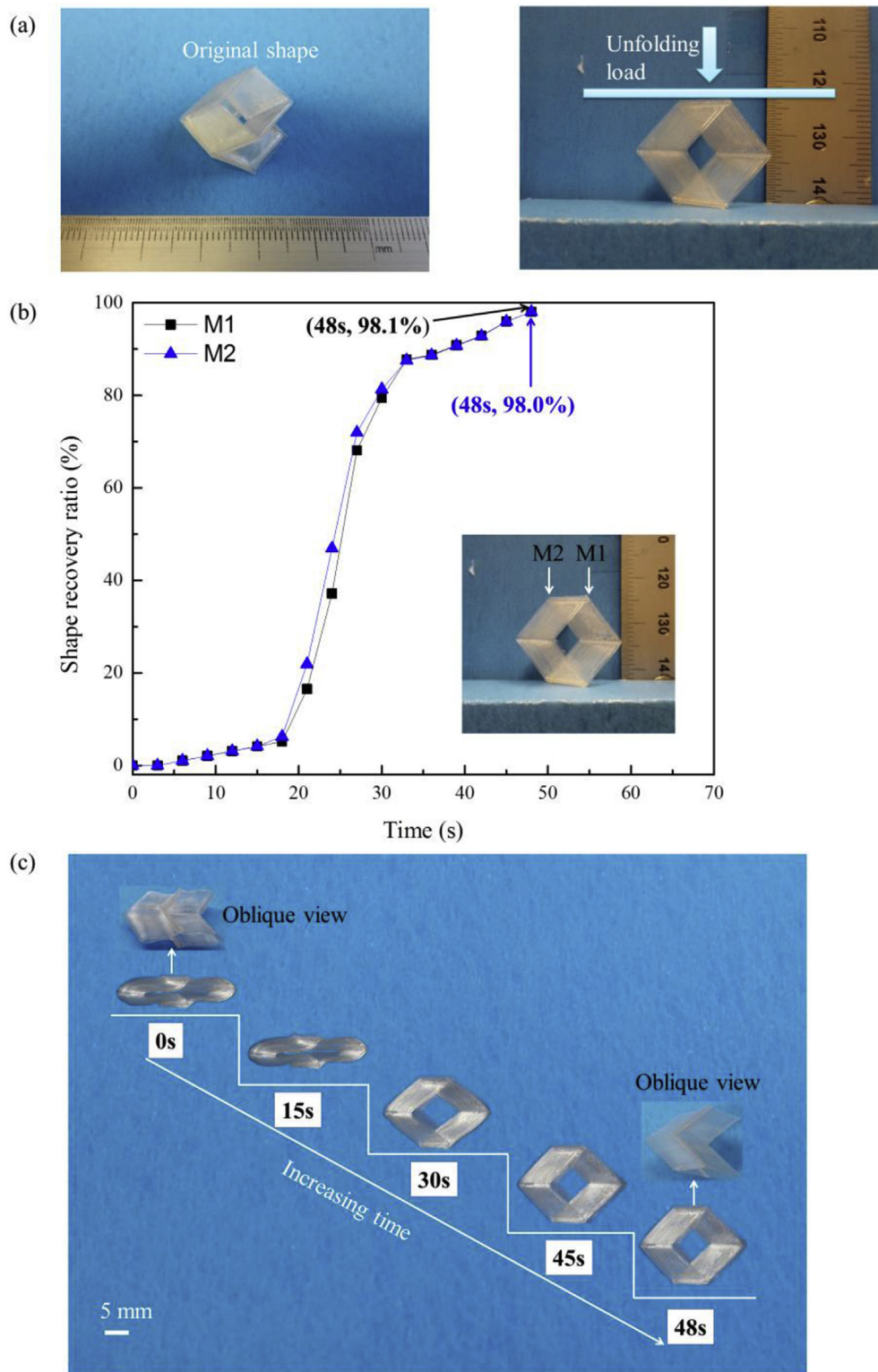
Fig. 6. Shape recovery behavior of a 4D printed Miura-origami tube subjected to an unfolding load. (a) The printed tube (left) is deformed by the unfolding load (right). (b) Shape recovery ratio vs. time curves for the heights of points M1 and M2. (c) Front view images of the shape recovery process of a specimen at 90 °C. Oblique views of the specimen at 0 s and 48 s are also shown.

4.2. Free shape recovery behavior

4.2.1. Miura-origami tessellation

The shape recovery cycle of a tessellation is shown in Fig. 4a. The specimen was first deformed to an intermediate shape under the unfolding load at the deformation temperature, T_d (higher than T_g), in an oven. The intermediate shape was maintained when the specimen was cooled down to the fixity temperature, T_f, and unloaded. Upon heating at the recovery temperature, T_r (higher than T_g), the specimen without external load recovered to nearly its original shape. During the shape recovery process, T_d and T_f were selected to be 90 °C and room temperature, respectively. The shape recovery history was recorded by a
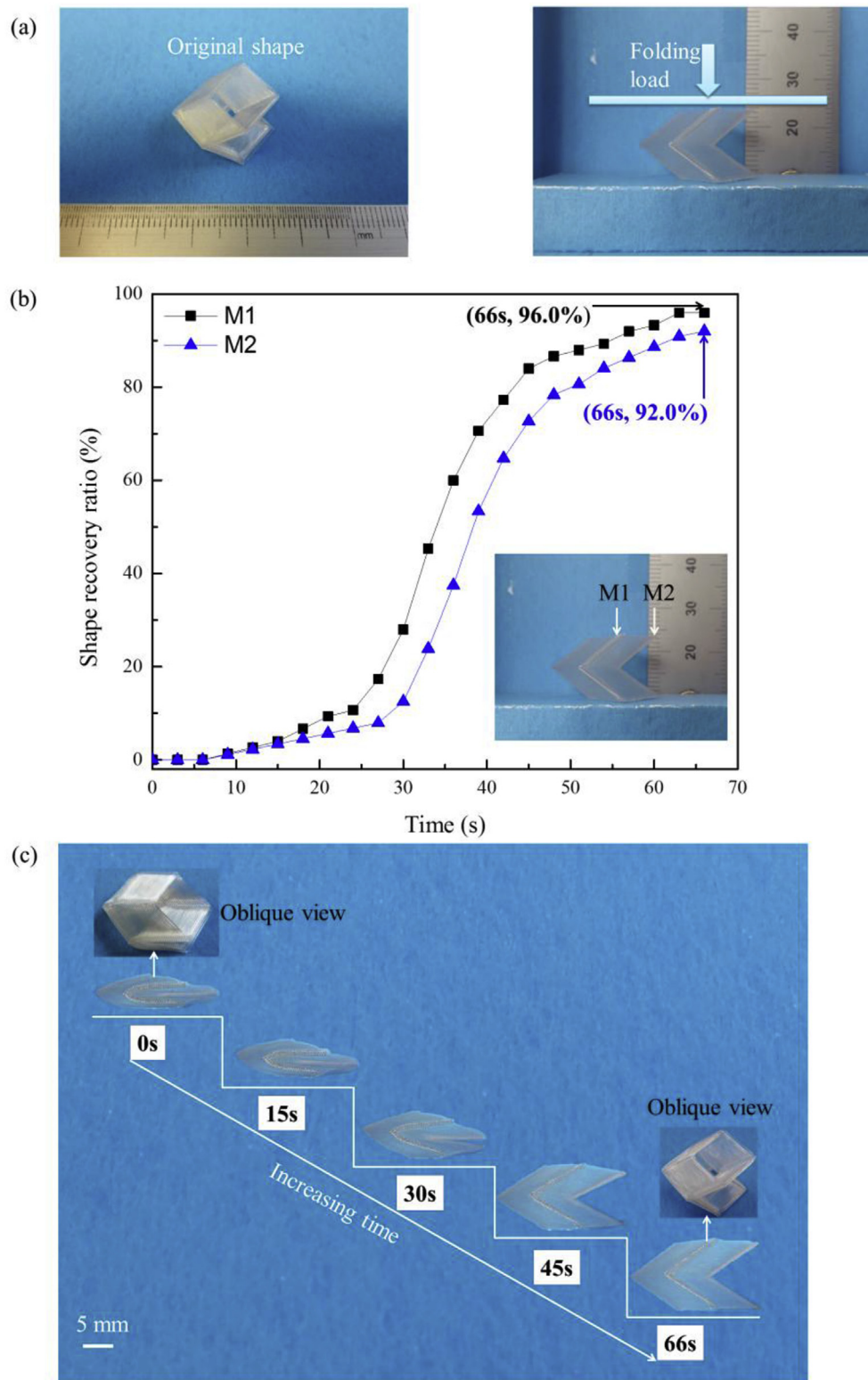
Fig. 7. Shape recovery behavior of a 4D printed Miura-origami tube subjected to a folding load. (a) The printed tube (left) is deformed by the folding load (right). (b) Shape recovery ratio vs. time curves for the heights of points M1 and M2. (c) Front view images of the shape recovery process of a specimen at 90 °C. Oblique views of the specimen at 0 s and 66 s are also shown.

video camera. The changes in the height of the points M1 and M2 of the specimen were recorded to calculate the shape recovery ratio. The shape recovery ratio (R_t) at shape recovery time t can be obtained using the following equation.

$$R_t(\%) = (h_t-h_i)/(h_o-h_i) \times 100 \qquad (1)$$

Here, h_t, h_i and h_o denote the height of the specimen at recovery time t, at the intermediate state and at the original state, respectively.

The effect of the recovery temperature on the shape recovery progression of a tessellation was studied at $T_r = 70\,°C$, $80\,°C$ and $90\,°C$, which were controlled by an oven. As shown on the left of Fig. 4b, the

Table 1
Specimen shape recovery data.

Specimen type	Type of loading	Shape recovery time (s)	Shape recovery ratio (%)	Volume change ratio (%)
Tessellation	unfolding	23.7 ± 1.5	97.9 ± 0.3	203.4 ± 6.2
Tessellation	folding	63.0 ± 3.0	95.6 ± 1.1	289.6 ± 5.6
Tube	unfolding	48.0 ± 3.0	97.5 ± 0.4	174.9 ± 1.3
Tube	folding	63.0 ± 3.0	94.8 ± 0.7	228.9 ± 5.7

time variation of shape recovery ratios are signified by the S-shaped curves with three different recovery stages. The deformed shape recovered slowly at the initial and final stages, and more rapidly during the middle stage. Also, at a given time, the shape recovery ratio increased with increasing recovery temperature. It can be seen that the shape recovery ratio curve at 70 °C showed lower shape recovery rate and final shape recovery ratio. The snapshots of the specimens at 15 s are shown on the right of Fig. 4b. The shape of specimen at 90 °C recovered the fastest among the three recovery temperatures. Although the difference between the shape recovery ratios at T_r = 80 °C and 90 °C is very slight, the specimen at T_r = 90 °C nearly recovered to its original

shape at 15 s. Therefore, the deformed specimen at higher recovery temperatures can recover faster to its original shape. As a result, the shape recovery temperature of 90 °C was selected for further studies of the shape recovery process.

The time variation of the front view of the tessellation specimen at 90 °C is shown in Fig. 4c. Starting as almost a flat 2D sheet at 0 s, the specimen folding motion actuated by heating can be clearly observed. The oblique view of the specimen at 22 s shows that the deformed shape dramatically recovered to its original shape. In addition, the specimen volume changes can also be observed during the shape recovery process. The volume change ratio (R_v) can be calculated by equation (2).

$$R_v(\%) = V_r/V_i \times 100 \qquad (2)$$

Here, the specimen volume is defined by the rectangular cubic volume as shown in Fig. 2. V_i and the V_r denote the specimen volumes at the intermediate state and at the recovered state, respectively. During the shape recovery process, the specimen average value of the volume change ratio of the deformed Miura-origami tessellation subjected to an unfolding load was up to 203.4%.

The shape recovery cycle of the 4D printed Miura-origami tessellation subjected to a folding load is shown in Fig. 5a. During the shape recovery process, the shape recovery ratio vs. time curves also
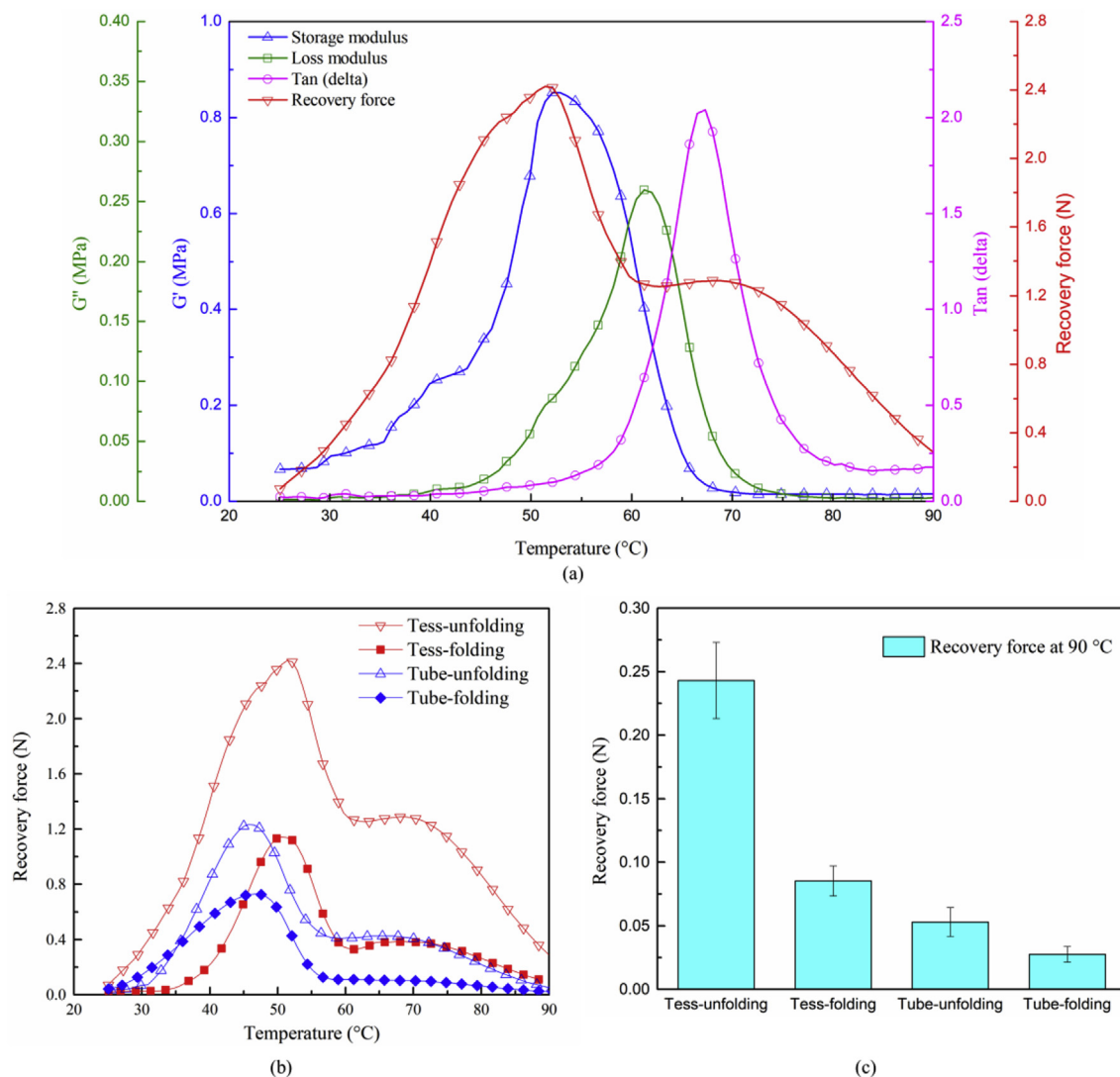
Fig. 8. (a) Thermomechanical properties and recovery force vs. temperature curves of a 4D printed Miura-origami tessellation subjected to an unfolding load. (b) Recovery force vs. temperature curves of a tessellation and a tube subjected to unfolding load and folding load. (c) Recovery forces at 90 °C with standard deviations. The legends Tess-unfolding and Tess-folding denote the tessellation subjected to an unfolding load and a folding load, respectively.
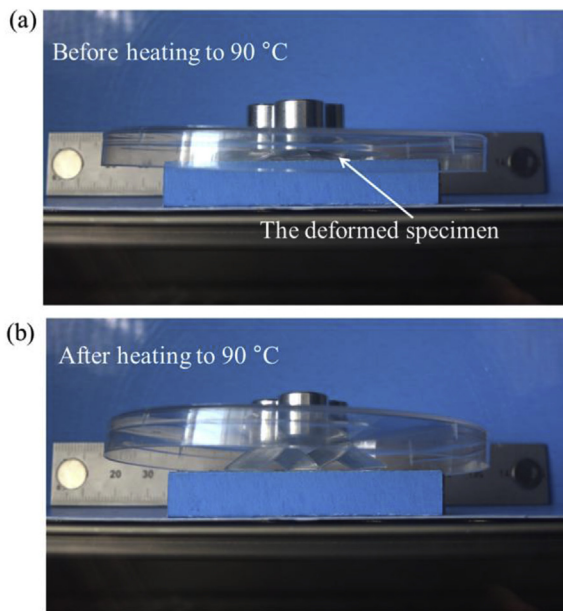
Fig. 9. Shape recovery capability of a Miura-origami tessellation. (a) The deformed specimen under a constant restraining weight placed on a platform. (b) After heating to 90 °C, the deformed specimen recovered to its original shape.

maintained an S-shape (Fig. 5b). The specimen heights at M1 and M2 were nearly unchanged after heating time of 63 s with the shape recovery ratios of 98.6% and 95.0%, respectively. The shape recovery time shown here was nearly three times as long as that subjected to an unfolding load at the recovery temperature of 90 °C (22 s). The reason of the difference is that the deformed specimen subjected to a folding load had a low recovery rate before 20 s due to the highly compacted and folded state. The specimen front views at various time intervals are shown in Fig. 5c. Starting at the highly folded state at 0 s, the specimen unfolding motion actuated by heating has been clearly demonstrated.

4.2.2. Miura-origami tube

The shape recovery behavior of the 4D printed Miura-origami tube subjected to an unfolding load is shown in Fig. 6. The shape recovery cycle here is the same as that adopted in Fig. 4a. Each unit cell in the tube unfolded when it was subjected to the compressive load along the arrow direction shown in Fig. 6a. The shape recovery ratio vs. time curves of the points M1 and M2 on the specimen were again S-shaped (Fig. 6b) with three distinct stages and a low recovery rate before 18 s. Also, the points M1 and M2 showed nearly identical recovery behavior and the shape recovery ratios of around 98% after heating time of 48 s. The recorded images of recovery of the deformed tube at 90 °C are shown in Fig. 6c from 0 s to 48 s. The inner space in the deformed tube was very small and it became larger with increasing time upon heating at 90 °C.

Similarly, the loading type, the shape recovery ratio vs. time curves and the specimen images at different times of a 4D printed Miura-origami tube subjected to a folding load have been studied and the results are shown in Fig. 7. The shape recovery cycle here was identical to that adopted in Fig. 5a. As can be seen in Fig. 7b, the deformed specimen had a low recovery rate before 24 s, which is longer than the corresponding time of 18 s observed in Fig. 6b. It can be seen that by comparing the results of Figs. 6 and 7, the deformed tube subjected to a folding load recovered to its original shape with longer time (66 s) than that subjected to an unfolding load (48 s).

The key parameters for evaluating the specimen free shape recovery properties are summarized in Table 1. The specimens subjected to an unfolding load showed shorter recovery times to their original shape and had slightly higher recovery ratios compared to those subjected to a

folding load. The above results were attributed to the different heat conduction rates. The specimens were compacted when subjected to a folding load, resulting in slower heating rates and recovery rates to the original shape. Furthermore, all specimens had distinct volume changes during the shape recovery process and the largest volume change ratio was up to 289.6%.

4.3. Constrained shape recovery behavior

Miura-origami tessellation as an example for test results based on DMA and DSC measurements are discussed first. Then results of recovery force measurements for the Miura-origami tessellation and tube are discussed. The shape recovery forces of the Miura-origami tessellation and tube were measured using the DMA compressive oscillatory experiments with the temperature ramp from 25 °C to 90 °C. The thermomechanical properties and recovery force vs. temperature curves of a Miura-origami tessellation subjected to an unfolding load are shown in Fig. 8a. The peak value of Tan (delta) occurred at 67 °C, which was regarded as the glass transition temperature (T_g) of the printed specimen. This value was close to the T_g of the SMP filament measured by DSC. The storage modulus decreased in the glass transition region from 52 °C to 67 °C. The recovery force first increased to its peak value of 2.42 N at 51 °C, and then it quickly decreased to 1.25 N at 63 °C. This result was consistent with the variation of storage modulus with temperature. The recovery force maintained a stable level from 63 °C to 67 °C and then it decreased to 0.26 N as temperature increases to 90 °C.

The recovery force vs. temperature curves of a tessellation and a tube subjected to unfolding load and folding load (Fig. 8b) show similar variations to those of Fig. 8a. Furthermore, the recovery forces of specimens at 90 °C are shown in Fig. 8c. The recovery forces of specimens subjected to an unfolding load are clearly larger than those subjected to a folding load.

Lastly, a Miura-origami tessellation subjected to an unfolding load was chosen to demonstrate its shape recovery capability under a constant restraining force (Fig. 9). The tessellation structure was selected because it showed the largest recovery force among all specimens studied (Fig. 8b). The constant restraining force was achieved by weight of 15.4 g on the deformed specimen (around 0.5 g). After heating to 90 °C, the deformed specimen was able to recover under the constant applied load (Fig. 9b).

5. Conclusions

In this study, the 4D printed thin-walled Miura-origami tessellations and tubes were fabricated using SMP filament and fused deposition modeling. Shape recovery behavior of the specimens subjected to unfolding load and folding load were investigated. The shape recovery temperature and the loading type had a significant effect on the shape memory behavior. The deformed specimens subjected to an unfolding load recovered to their original shapes faster than those subjected to a folding load, which was attributed to the different heat conduction rates. Besides, the recovery forces of the specimens subjected to an unfolding load exhibited larger values comparing to those subjected to a folding load. The large volume changes during the shape recovery process indicated the potential of utilizing 4D printed origami structures for space-saving devices. Lastly, the shape recovery capability of a Miura-origami structure under a constant restraining force has been demonstrated.

Acknowledgements

References

[1] Dudte LH, Vouga E, Tachi T, Mahadevan L. Programming curvature using origami tessellations. Nat Mater 2016;15:583–8.

[2] Miura K. Triangles and quadrangles in space. Proceedings of the international association for shell and spatial structures symposium. 2009. p. 27–38. Valencia, October.

[3] Gattas JM, Wu W, You Z. Miura-base rigid origami: parameterizations of first-level derivative and piecewise geometries. J Mech Des 2013;135(11):111011.

[4] Song K, Zhou X, Zang S, Wang H, You Z. Design of rigid-foldable doubly curved origami tessellations based on trapezoidal crease patterns. Proc R Soc A 2017;473:20170016.

[5] Callens SJP, Zadpoor AA. From flat sheets to curved geometries: origami and kirigami approaches. Mater Today 2018;21(3):241–64.

[6] Kamrava S, Mousanezhad D, Ebrahimi H, Ghosh R, Vaziri A. Origami-based cellular metamaterial with auxetic, bistable, and self-locking properties. Sci Rep 2017;7:46046.

[7] Yasuda H, Yang J. Reentrant origami-based metamaterials with negative Poisson's ratio and bistability. Phys Rev Lett 2015;114(18):185502.

[8] Schenk M, Guest SD. Geometry of miura-folded metamaterials. Proc Natl Acad Sci USA 2013;110(9):3276–81.

[9] Filipov ET, Tachi T, Paulino GH. Origami tubes assembled into stiff, yet reconfigurable structures and metamaterials. Proc Natl Acad Sci USA 2015;112(40):12321–6.

[10] Li S, Vogt DM, Rus D, Wood RJ. Fluid-driven origami-inspired artificial muscles. Proc Natl Acad Sci USA 2017;114(50):13132–7.

[11] Nishiyama Y. Miura folding: applying origami to space exploration. Int J Pure Appl Math 2012;79(2):269–79.

[12] Quan Z, Wu A, Keefe M, Qin X, Yu J, Suhr J, Byun J-H, Kim B-S, Chou T-W. Additive manufacturing of multi-directional preforms for composites: opportunities and challenges. Mater Today 2015;18(9):503–12.

[13] Ngo TD, Kashani A, Imbalzano G, Nguyen KTQ, Hui D. Additive manufacturing (3D printing): a review of materials, methods, applications and challenges. Compos Part B Eng 2018;143:172–96.

[14] Tibbits S. 4D printing: multi-material shape change. Archit Design 2014;84(1):116–21.

[15] Ge Q, Dunn CK, Qi HJ, Dunn ML. Active origami by 4D printing. Smart Mater Struct 2014;23(9):094007.

[16] Mao Y, Yu K, Isakov MS, Wu J, Dunn ML, Qi HJ. Sequential self-folding structures by 3D printed digital shape memory polymers. Sci Rep 2015;5:13616.

[17] Wagner M, Chen T, Shea K. Large shape transforming 4D auxetic structures. 3D Print Addit Manuf 2017;4(3):133–42.

[18] Leist SK, Zhou J. Current status of 4D printing technology and the potential of light-reactive smart materials as 4D printable materials. Virtual Phys Prototyp 2016;11(4):249–62.

[19] Gladman AS, Matsumoto EA, Nuzzo RG, Mahadevan L, Lewis JA. Biomimetic 4D printing. Nat Mater 2016;15:413–8.

[20] Zhao Q, Qi HJ, Xie T. Recent progress in shape memory polymer: new behavior, enabling materials, and mechanistic understanding. Prog Polym Sci 2015;49–50:79–120.

[21] Wang X, Sparkman J, Gou J. Electrical actuation and shape memory behavior of polyurethane composites incorporated with printed carbon nanotube layers.

Compos Sci Technol 2017;141:8–15.

[22] Wei H, Zhang Q, Yao Y, Liu L, Liu Y, Leng J. Direct-write fabrication of 4D active shape-changing structures based on a shape memory polymer and its nanocomposite. ACS Appl Mater Interfaces 2017;9(1):876–83.

[23] Miao S, Castro N, Nowicki M, Xia L, Cui H, Zhou X, Zhu W, Lee S-J, Sarkar K, Vozzi G, Tabata Y, Fisher J, Zhang LG. 4D printing of polymeric materials for tissue and organ regeneration. Mater Today 2017;20(10):577–91.

[24] Zarek M, Mansour N, Shapira S, Cohn D. 4D printing of shape memory-based personalized endoluminal medical devices. Macromol Rapid Commun 2017;38(2):1600628.

[25] Zarek M, Layani M, Cooperstein I, Sachyani E, Cohn D, Magdassi S. 3D printing of shape memory polymers for flexible electronic devices. Adv Mater 2016;28(22):4449–54.

[26] Zarek M, Layani M, Eliazar S, Mansour N, Cooperstein I, Shukrun E, Szlar A, Cohn D, Magdassi S. 4D printing shape memory polymers for dynamic jewellery and fashionwear. Virtual Phys Prototyp 2016;11(4):263–70.

[27] Leist SK, Gao D, Chiou R, Zhou J. Investigating the shape memory properties of 4D printed polylactic acid (PLA) and the concept of 4D printing onto nylon fabrics for the creation of smart textiles. Virtual Phys Prototyp 2017;12(4):290–300.

[28] van Manen T, Janbaz S, Zadpoor AA. Programming 2D/3D shape-shifting with hobbyist 3D printers. Mater Horiz 2017;4:1064–9.

[29] Yu K, Ritchie A, Mao Y, Dunn ML, Qi HJ. Controlled sequential shape changing components by 3D printing of shape memory polymer multimaterials. Procedia IUTAM 2015;12:193–203.

[30] Teoh JEM, Zhao Y, An J, Chua CK, Liu Y. Multi-stage responsive 4D printed smart structure through varying geometric thickness of shape memory polymer. Smart Mater Struct 2017;26(12):125001.

[31] Bodaghi M, Damanpack AR, Liao WH. Adaptive metamaterials by functionally graded 4D printing. Mater Des 2017;135:26–36.

[32] Ge Q, Dunn CK, Qi HJ, Dunn ML. Active origami by 4D printing. Smart Mater Struct 2014;23(9):094007.

[33] Yuan C, Wang T, Dunn ML, Qi HJ. 3D printed active origami with complicated folding patterns. Int J Precis Eng Manuf 2017;4(3):281–9.

[34] Teoh JEM, An J, Feng X, Zhao Y, Chua CK, Liu Y. Design and 4D printing of cross-folded origami structures: a preliminary investigation. Materials 2018;11(3):376.

[35] Volk BL, Lagoudas DC, Maitland DJ. Characterizing and modeling the free recovery and constrained recovery behavior of a polyurethane shape memory polymer. Smart Mater Struct 2011;20:094004.

[36] Du H, Liu L, Zhang F, Zhao W, Leng J, Liu Y. Thermal-mechanical behavior of styrene-based shape memory polymer tubes. Polym Testing 2017;57:119–25.

[37] Senatov FS, Zadorozhnyy MY, Niaza KV, Medvedev VV, Kaloshkin SD, Anisimova NY, Kiselevskiy MV, Yang K-C. Shape memory effect in 3D-printed scaffolds for self-fitting implants. Eur Polym J 2017;93:222–31.

[38] Chen L, Li W, Liu Y, Leng J. Epoxy shape-memory polymer reinforced by thermally reduced graphite oxide: influence of processing techniques. J Appl Polym Sci 2015;132(38):42502.

[39] Mousanezhad D, Kamrava S, Vaziri A. Origami-based building blocks for modular construction of foldable structures. Sci Rep 2017;7:14792.

[40] Zhang W, Zhang F, Lan X, Leng J, Wu AS, Bryson TM, Cotton C, Gu B, Sun B, Chou T-W. Shape memory behavior and recovery force of 4D printed textile functional composites. Compos Sci Technol 2018;160:224–30.